CLEO CONF 97-30
EPS97 343

A New Measurement of the $b \to u$ Semileptonic Decays $B \to \rho\ell\nu$ and $B \to \omega\ell\nu$

CLEO Collaboration

(August 14, 1997)

Abstract

We report preliminary results of a new measurement of the branching fractions $B^0 \to \rho^-\ell^+\nu$, $B^+ \to \rho^0\ell^+\nu$, and $B^+ \to \omega\ell^+\nu$ at CLEO. We find $\mathcal{B}(B^0 \to \rho^-\ell^+\nu) = (2.0\pm0.3\pm0.3)\times10^{-4}$ using the ISGW2 model to calculate the signal efficiencies. We assume no $B \to \pi\pi\ell\nu$ nonresonant contribution, and use isospin and quark model considerations to fix the relative normalizations of the ρ^-, ρ^0, and ω modes. These results are in good agreement with, and largely statistically independent of, measurements previously published by CLEO.

M. Artuso,[1] A. Efimov,[1] M. Goldberg,[1] D. He,[1] S. Kopp,[1] G. C. Moneti,[1] R. Mountain,[1] S. Schuh,[1] T. Skwarnicki,[1] S. Stone,[1] G. Viehhauser,[1] X. Xing,[1] J. Bartelt,[2] S. E. Csorna,[2] V. Jain,[2,*] K. W. McLean,[2] S. Marka,[2] R. Godang,[3] K. Kinoshita,[3] I. C. Lai,[3] P. Pomianowski,[3] S. Schrenk,[3] G. Bonvicini,[4] D. Cinabro,[4] R. Greene,[4] L. P. Perera,[4] G. J. Zhou,[4] B. Barish,[5] M. Chadha,[5] S. Chan,[5] G. Eigen,[5] J. S. Miller,[5] C. O'Grady,[5] M. Schmidtler,[5] J. Urheim,[5] A. J. Weinstein,[5] F. Würthwein,[5] D. W. Bliss,[6] G. Masek,[6] H. P. Paar,[6] S. Prell,[6] V. Sharma,[6] D. M. Asner,[7] J. Gronberg,[7] T. S. Hill,[7] D. J. Lange,[7] S. Menary,[7] R. J. Morrison,[7] H. N. Nelson,[7] T. K. Nelson,[7] C. Qiao,[7] J. D. Richman,[7] D. Roberts,[7] A. Ryd,[7] M. S. Witherell,[7] R. Balest,[8] B. H. Behrens,[8] W. T. Ford,[8] H. Park,[8] J. Roy,[8] J. G. Smith,[8] J. P. Alexander,[9] C. Bebek,[9] B. E. Berger,[9] K. Berkelman,[9] K. Bloom,[9] D. G. Cassel,[9] H. A. Cho,[9] D. S. Crowcroft,[9] M. Dickson,[9] P. S. Drell,[9] K. M. Ecklund,[9] R. Ehrlich,[9] A. D. Foland,[9] P. Gaidarev,[9] L. Gibbons,[9] B. Gittelman,[9] S. W. Gray,[9] D. L. Hartill,[9] B. K. Heltsley,[9] P. I. Hopman,[9] J. Kandaswamy,[9] P. C. Kim,[9] D. L. Kreinick,[9] T. Lee,[9] Y. Liu,[9] G. S. Ludwig,[9] N. B. Mistry,[9] C. R. Ng,[9] E. Nordberg,[9] M. Ogg,[9,†] J. R. Patterson,[9] D. Peterson,[9] D. Riley,[9] A. Soffer,[9] B. Valant-Spaight,[9] C. Ward,[9] M. Athanas,[10] P. Avery,[10] C. D. Jones,[10] M. Lohner,[10] C. Prescott,[10] J. Yelton,[10] J. Zheng,[10] G. Brandenburg,[11] R. A. Briere,[11] A. Ershov,[11] Y. S. Gao,[11] D. Y.-J. Kim,[11] R. Wilson,[11] H. Yamamoto,[11] T. E. Browder,[12] Y. Li,[12] J. L. Rodriguez,[12] T. Bergfeld,[13] B. I. Eisenstein,[13] J. Ernst,[13] G. E. Gladding,[13] G. D. Gollin,[13] R. M. Hans,[13] E. Johnson,[13] I. Karliner,[13] M. A. Marsh,[13] M. Palmer,[13] M. Selen,[13] J. J. Thaler,[13] K. W. Edwards,[14] A. Bellerive,[15] R. Janicek,[15] D. B. MacFarlane,[15] P. M. Patel,[15] A. J. Sadoff,[16] R. Ammar,[17] P. Baringer,[17] A. Bean,[17] D. Besson,[17] D. Coppage,[17] C. Darling,[17] R. Davis,[17] N. Hancock,[17] S. Kotov,[17] I. Kravchenko,[17] N. Kwak,[17] S. Anderson,[18] Y. Kubota,[18] S. J. Lee,[18] J. J. O'Neill,[18] S. Patton,[18] R. Poling,[18] T. Riehle,[18] V. Savinov,[18] A. Smith,[18] M. S. Alam,[19] S. B. Athar,[19] Z. Ling,[19] A. H. Mahmood,[19] H. Severini,[19] S. Timm,[19] F. Wappler,[19] A. Anastassov,[20] J. E. Duboscq,[20] D. Fujino,[20,‡] K. K. Gan,[20] T. Hart,[20] K. Honscheid,[20] H. Kagan,[20] R. Kass,[20] J. Lee,[20] M. B. Spencer,[20] M. Sung,[20] A. Undrus,[20,§] R. Wanke,[20] A. Wolf,[20] M. M. Zoeller,[20] B. Nemati,[21] S. J. Richichi,[21] W. R. Ross,[21] P. Skubic,[21] M. Bishai,[22] J. Fast,[22] J. W. Hinson,[22] N. Menon,[22] D. H. Miller,[22] E. I. Shibata,[22] I. P. J. Shipsey,[22] M. Yurko,[22] S. Glenn,[23] S. D. Johnson,[23] Y. Kwon,[23,**] S. Roberts,[23] E. H. Thorndike,[23] C. P. Jessop,[24] K. Lingel,[24] H. Marsiske,[24] M. L. Perl,[24] D. Ugolini,[24] R. Wang,[24] X. Zhou,[24] T. E. Coan,[25] V. Fadeyev,[25] I. Korolkov,[25] Y. Maravin,[25] I. Narsky,[25] V. Shelkov,[25] J. Staeck,[25] R. Stroynowski,[25] I. Volobouev,[25] and J. Ye[25]

[*]Permanent address: Brookhaven National Laboratory, Upton, NY 11973.

[†]Permanent address: University of Texas, Austin TX 78712

[‡]Permanent address: Lawrence Livermore National Laboratory, Livermore, CA 94551.

[§]Permanent address: BINP, RU-630090 Novosibirsk, Russia.

[**]Permanent address: Yonsei University, Seoul 120-749, Korea.

[1]Syracuse University, Syracuse, New York 13244
[2]Vanderbilt University, Nashville, Tennessee 37235
[3]Virginia Polytechnic Institute and State University, Blacksburg, Virginia 24061
[4]Wayne State University, Detroit, Michigan 48202
[5]California Institute of Technology, Pasadena, California 91125
[6]University of California, San Diego, La Jolla, California 92093
[7]University of California, Santa Barbara, California 93106
[8]University of Colorado, Boulder, Colorado 80309-0390
[9]Cornell University, Ithaca, New York 14853
[10]University of Florida, Gainesville, Florida 32611
[11]Harvard University, Cambridge, Massachusetts 02138
[12]University of Hawaii at Manoa, Honolulu, Hawaii 96822
[13]University of Illinois, Champaign-Urbana, Illinois 61801
[14]Carleton University, Ottawa, Ontario, Canada K1S 5B6
and the Institute of Particle Physics, Canada
[15]McGill University, Montréal, Québec, Canada H3A 2T8
and the Institute of Particle Physics, Canada
[16]Ithaca College, Ithaca, New York 14850
[17]University of Kansas, Lawrence, Kansas 66045
[18]University of Minnesota, Minneapolis, Minnesota 55455
[19]State University of New York at Albany, Albany, New York 12222
[20]Ohio State University, Columbus, Ohio 43210
[21]University of Oklahoma, Norman, Oklahoma 73019
[22]Purdue University, West Lafayette, Indiana 47907
[23]University of Rochester, Rochester, New York 14627
[24]Stanford Linear Accelerator Center, Stanford University, Stanford, California 94309
[25]Southern Methodist University, Dallas, Texas 75275

I. INTRODUCTION

The study of exclusive semileptonic $b \to u\ell\nu$ decays is an active area of both theoretical and experimental study. The decay $B \to \rho\ell\nu$ provides a way to measure $|V_{ub}|$. The measurement of $b \to u\ell\nu$ branching fractions relies on the theoretical prediction of kinematical distributions; the extraction of $|V_{ub}|$ depends on the absolute normalization of theoretical predictions as well. Calculations including quark models [1] [2], lattice QCD [3], and QCD sum rules [4] have been used to predict $|V_{ub}|$ using $B \to \rho\ell\nu$ and $B \to \pi\ell\nu$.

CLEO [5] has previously observed the decays $B^0 \to \rho^-\ell^+\nu$, $B^+ \to \rho^0\ell^+\nu$, $B^+ \to \omega\ell^+\nu$, $B^0 \to \pi^-\ell^+\nu$, and $B^+ \to \pi^0\ell^+\nu$ (charge conjugate modes are implied throughout this paper) by measuring both the missing energy and momentum to infer the momentum of the neutrino. This method obtained the measurements

$$\mathcal{B}(B^0 \to \rho^-\ell^+\nu) = (2.5 \pm 0.4^{+0.3}_{-0.4} \pm 0.5) \times 10^{-4}, \tag{1}$$

$$\mathcal{B}(B^0 \to \pi^-\ell^+\nu) = (1.8 \pm 0.4 \pm 0.3 \pm 0.2) \times 10^{-4}, \tag{2}$$

$$|V_{ub}| = (3.3 \pm 0.2^{+0.3}_{-0.4} \pm 0.7) \times 10^{-3}, \tag{3}$$

where the errors are statistical, systematic, and for model dependence.

We report on a new analysis method for $B \to \rho\ell\nu$, which is sensitive primarily to leptons with energies above the $b \to c\ell\nu$ lepton energy endpoint. Having a higher signal efficiency as well as higher backgrounds, this analysis is largely statistically independent of previous results.

II. DATA SAMPLE

The data used in this analysis were hadronic events produced at the Cornell Electron Storage Ring (CESR) and collected by the CLEO-II detector. An integrated luminosity of 3.13 fb^{-1} was accumulated on the $\Upsilon(4S)$ resonance, corresponding to 3.3×10^6 $B\overline{B}$ pairs. Additionally, data collected at a center of mass energy approximately 60 MeV below the $\Upsilon(4S)$ resonance are utilized to study the background from continuum events at the $\Upsilon(4S)$.

The CLEO-II detector [8] accurately measures both charged and neutral particles over the majority of the 4π solid angle. Three concentric cylindirical wire chambers, in a 1.5 Tesla magnetic field, cover 94% of the solid angle and provide a total momentum resolution of $\frac{\Delta p}{p} \approx 0.6\%$ for $p = 2.0$ GeV/c. A CsI electromagnetic calorimeter covers 98% of the solid angle, and provides excellent resolution for the reconstruction of photons and π^0s.

III. EVENT SELECTION

Tracking and calorimeter measurements, along with specific ionization (dE/dx) information are combined to identify electron candidates. This analysis makes use of electrons with energies above 1.7 GeV, and with $|\cos\theta| \leq 0.85$, where θ is the polar angle measured with respect to the beam axis. Electron identification efficiency is above 90% for the momentum range of interest. The probability of a hadron being misidentified as an electron is approximately 0.1%.

Muon candidates are required to traverse at least 7 interaction lengths of iron, again with $|\cos\theta| \leq 0.85$. The efficiency for identifying muons with $E_\mu \geq 2.2$ GeV is 85%, with a fake rate of approximately 0.4%.

Candidate π^0s are selected from $\gamma\gamma$ pairs which have a reconstructed mass within 2.5σ of the nominal π^0 mass. To make up a π^0, CsI clusters must be consistent with not being a split-off from a charged track. Additionally, clusters must have $E_\gamma \geq 30$ MeV, and π^0s must satisfy $E_{\pi^0} \geq 325$ MeV.

The $\rho^\pm$, ρ^0, and ω candidates are reconstructed in $\pi^\pm\pi^0$, $\pi^+\pi^0$, and $\pi^+\pi^-\pi^0$ final states respectively. Candidates are required to have a momentum greater than 700 MeV/c. Combinatoric background is suppressed in the ω mode by making a cut on the $\omega \to \pi^+\pi^-\pi^0$ Dalitz amplitude.

In addition to $\rho\ell$ and $\omega\ell$ candidates, we consider $\pi^\pm\ell$ and $\pi^0\ell$ candidates in order to better understand the $B \to \pi\ell\nu$ background. We do not quote $\mathcal{B}(B \to \pi\ell\nu)$ results at this time.

We separate leptons into three lepton-energy bins. We are most sensitive to leptons with energies between 2.3 GeV and 2.7 GeV (the HILEP region). We also examine candidate leptons between 2.0 GeV and 2.3 GeV (LOLEP), as well as between 1.7 GeV and 2.0 GeV.

For leptons beyond the $b \to c\ell\nu$ lepton energy endpoint, the continuum is the dominant source of background events. At the Υ(4S), B mesons are produced nearly at rest ($\beta \approx 0.065$), and their decay products are uniformly distributed in solid angle. Continuum events tend to be more jet-like in shape. We select "spherical" events in several ways:

- The ratio of the second to zeroth Fox-Wolfram [6] moments is requied to be less than 0.3.
- $\rho\ell$, $\omega\ell$ and $\pi\ell$ candidates are required to have $|\cos\theta_{\rm thrust}| \leq 0.8$, where $\theta_{\rm thrust}$ is defined to be the angle between the thrust axis of the candidate and the thrust axis of the rest of the event.
- We select events with $|\cos\theta_\nu| \leq 0.9$, where θ_ν is the polar angle of the missing momentum with respect to the beam axis.
- Events whose energy is evenly distributed around the momentum axis of the candidate lepton are chosen using a Fisher discriminant [7]. $B\overline{B}$ events tend to be more evenly distributed in $\cos\theta$ cones around the candidate lepton than jetty continuum events.

We also suppress background by using the kinematics of $B \to \rho(\omega,\pi)\ell\nu$ decay. Using the constraint $E_B = E_{\rm beam}$, we reconstruct the angle between the B momentum direction and that of the $\Upsilon \equiv \rho(\omega,\pi) + \ell$ system.

$$\cos\theta_{\rm BY} \equiv \frac{m_{\rm B}^2 + m_{\rho\ell}^2 - 2E_{\rm B}E_{\rho\ell}}{2|\vec{p}_{\rm B}||\vec{p}_{\rho\ell}|} \tag{4}$$

We require that $|\cos\theta_{\rm BY}| \leq 1.0$.

Using all tracks and clusters found in the event, we define

$$\vec{p}_{\rm miss} \equiv -\Sigma\vec{p}_{\rm i}. \tag{5}$$

We require that the angle between $\vec{p}_{\rm miss}$ and the neutrino candidate inferred using the $\rho+\ell$ candidate be small, less than 0.6 radians. As only the magnitude of the B momentum is known (from the beam energy constraint), there is an azimuthal ambiguity on the direction of the inferred neutrino. The solution which minimizes the angle with $\vec{p}_{\rm miss}$ is taken.

Finally, we calculate

$$\Delta E \equiv E_\rho + E_\ell + |\vec{p}_{\rm miss}| - E_{\rm beam}. \tag{6}$$

For signal events, we should find that $\Delta E = 0$, within experimental resolution.

Each event that satisfies the cuts listed above is allowed to enter only one signal channel ($\rho^\pm\ell\nu$, $\rho^0\ell\nu$, $\omega\ell\nu$, $\pi^\pm\ell\nu$, or $\pi^0\ell\nu$). The channel selected is the one in which the reconstructed value of the B meson mass is closest to the nominal B mass.

IV. FITTING TECHNIQUE

We perform a two-dimensional-maximum likelihood fit in $M(\pi\pi)$ vs. ΔE, $M(\pi^+\pi^-\pi^0)$ vs. ΔE, and ΔE in the three lepton-energy bins, using MINUIT [11], for $\rho-\ell$, $\omega-\ell$ and $\pi-\ell$ candidates respectively. We constrain the relative normalizations of $B^0 \to \rho^-\ell^+\nu$, $B^+ \to \rho^0\ell^+\nu$, and $B^+ \to \omega\ell^+\nu$ as well as $B^0 \to \pi^-\ell^+\nu$ to $B^+ \to \pi^0\ell^+\nu$ using the isospin and quark model relations [9]

$$\Gamma(B^0 \to \rho^-\ell^+\nu) = 2\times\Gamma(B^+ \to \rho^0\ell^+\nu), \tag{7}$$
$$\Gamma(B^0 \to \rho^-\ell^+\nu) = 2\times\Gamma(B^+ \to \omega\ell^+\nu), \tag{8}$$
$$\Gamma(B^0 \to \pi^-\ell^+\nu) = 2\times\Gamma(B^+ \to \pi^0\ell^+\nu). \tag{9}$$

We use a GEANT [10] based full detector simulation and a detailed model of B and D decays to model the shapes of the $M(\pi\pi(\pi))$ vs. ΔE distributions for $B\to\rho\ell\nu$, $B\to\omega\ell\nu$, $B\to\pi\ell\nu$, $b\to c\ell\nu$, and other $b\to u\ell\nu$ events. The ISGW2 [1] model is used to simulate feeddown from $b\to u\ell\nu$ modes, including resonances up to the $\rho(1450)$.

The fit is used to determine the normalization of

- $B\to\rho\ell\nu$ events, including crossfeed events. The crossfeed contribution corresponds to events from one vector mode passing the selection cuts of another vector mode. $\rho^\pm\ell\nu \leftrightarrow \rho^0\ell\nu$ and $\rho\ell\nu \leftrightarrow \omega\ell\nu$ are crossfeeds.

- $B \to \pi \ell \nu$ events.
- $b \to u \ell \nu$ feeddown events. Feeddown events include all $B \to X_u \ell \nu$ contributions other than ρ and π. One normalization parameter is used in each of three lepton-energy bins.
- $b \to c \ell \nu$ events. One normalization parameter in each of five modes.

For each source of events, except for the $b \to u \ell \nu$ feeddown contribution, the relative number of events in each lepton-energy bin is fixed from Monte Carlo. The normalization of the feeddown contribution is allowed to float separately in each lepton energy bin, as theory does not include predictions of all of the $b \to u \ell \nu$ modes present in the lower lepton-energy bins.

The off-resonance data are used to predict the contribution from continuum events in the fit. Additionally, the normalization and the shape of the $M(\pi\pi)$ vs. ΔE distribution of the small number of events containing a hadron identified as an electron or muon are determined using data.

V. RESULTS

Table I summarizes the results for the vector modes in the HILEP and LOLEP lepton-energy bins. A clear excess over the expected number of events from the continuum and $b \to c \ell \nu$ backgrounds is seen in both HILEP and LOLEP.

As explained above, we use the Monte Carlo to describe the relative number of $b \to c \ell \nu$ events in each lepton-energy bin. In this way, the $b \to c \ell \nu$ contribution in HILEP is largely determined by the lower lepton-energy bins. The systematic error associated with doing this is not large, as our $b \to c \ell \nu$ backgrounds come from well understood, low multiplicity modes such as $B \to D^* \ell \nu$ and $B \to D \ell \nu$. We expect approximately two $B \to D^{**} \ell \nu$ events in HILEP. In LOLEP, more than 90% of the events passing all cuts in the $b \to c \ell \nu$ Monte Carlo are either $B \to D^* \ell \nu$ or $B \to D \ell \nu$.

Figures 1 through 6 show projections of the fit. The ISGW2 model is used to describe the distributions for the $B \to \rho \ell \nu$, $B \to \pi \ell \nu$, and $b \to u \ell \nu$ feeddown contributions. The off-resonance data, scaled by the relative integrated luminosity, is subtracted.

Figure 1 shows the HILEP $M(\pi\pi)$ distribution for events with $\Delta E \geq -0.2$ GeV. A clear excess is seen over the expected contribution from $b \to c \ell \nu$ events. Figure 2 shows the ΔE distribution for events within ± 150 MeV of the nominal ρ mass. We do not currently understand the systematic excess of observed events for $\Delta E \leq 0.0$ GeV. Changing the normalization of $b \to c \ell \nu$ events in HILEP relative to LOLEP does not account for this excess in a manner consistent with the lepton energy distribution shown in Figure 6. Figure 3 shows the q^2 distribution for events with $\Delta E \geq -0.2$ GeV.

The $M(\pi^+\pi^-\pi^0)$ distribution, shown in Figure 4, is consistent with expectations from the $\rho^\pm$ and ρ^0 modes. We are not sensitive to $B \to \omega\ell\nu$ alone.

The LOLEP $M(\pi\pi)$ and ΔE projections are shown in Figure 5. Again there is a clear excess over the $b \to c\ell\nu$ contribution. The peak in $M(\pi\pi)$ around 1.7 GeV/c^2, consists of $b \to c\ell\nu$ events where a D decays to $K\pi$. This peak is below the nominal M_D as we have misreconstructed the K as a π. Figure 6 shows the lepton energy distribution for events with $M(\pi\pi)$ within ±150 MeV of the nominal ρ mass, and with $\Delta E \geq -0.2$ GeV.

Figure 7 shows $M(\pi\pi)$ distributions in HILEP and LOLEP for events with $\Delta E \leq -0.2$ GeV. Also shown are ΔE projections where $M(\pi\pi)$ is required to be outside of ±150 MeV of the nominal ρ mass. The agreement in these plots again shows that the background is well understood both in HILEP and in LOLEP. The fit also agrees well with the data for $1.7 \leq E_\ell \leq 2.0$ GeV.

Using the ISGW2 model to obtain signal efficiencies, we find

$$\mathcal{B}(B^0 \to \rho^-\ell^+\nu) = (2.0 \pm 0.3) \times 10^{-4} \qquad \text{(ISGW2)}, \tag{10}$$

where the error is statistical only.

	$\rho^\pm$ HI	ρ^0 HI	ω HI	$\rho^\pm$ LO	ρ^0 LO	ω LO
Υ(4S) yield	193	506	358	2106	6374	7128
Continuum bkg.	55 ± 10	189 ± 19	189 ± 19	113 ± 15	337 ± 26	282 ± 24
$b \to c\ell\nu$ bkg.	32 ± 1	104 ± 1	69 ± 1	1783 ± 26	5548 ± 48	6604 ± 52
fake lepton bkg.	4 ± 2	13 ± 7	10 ± 5	12 ± 6	35 ± 18	41 ± 21
$b \to u\ell\nu$ feeddown bkg.	21 ± 8	45 ± 18	33 ± 14	113 ± 27	237 ± 56	259 ± 61
$B \to \pi\ell\nu$ bkg.	11 ± 3	20 ± 5	3 ± 1	17 ± 4	34 ± 8	7 ± 2
Crossfeed yield	17 ± 3	63 ± 10	26 ± 4	16 ± 3	65 ± 11	41 ± 7
Fit signal yield	54 ± 9	55 ± 9	20 ± 3	51 ± 8	56 ± 9	24 ± 4
Signal Efficiency (ISGW2)	0.041	0.083	0.033	0.039	0.085	0.040

TABLE I. Summary of data yields for the $\rho^\pm$, ρ^0, and ω modes with lepton energies between 2.3 and 2.7 GeV (HILEP) and between 2.0 and 2.3 GeV (LOLEP). The crossfeed contribution corresponds to events from one vector mode passing the selection cuts of another vector mode ($\rho^0\ell\nu \leftrightarrow \rho^\pm\ell\nu$ or $\rho\ell\nu \leftrightarrow \omega\ell\nu$) and is constrained to the signal in the fit. The $b \to u\ell\nu$ background includes all $B \to X_u\ell\nu$ modes except for ρ, ω and π. All errors are statistical only. Errors on the fitted signal yield and crossfeed background are completely correlated, as are the errors on the $B \to \pi\ell\nu$ events. Errors on the $b \to c\ell\nu$ background are correlated between HILEP and LOLEP, but are not correlated mode to mode. Errors on the $b \to u\ell\nu$ feeddown are completely correlated between modes, but not between HILEP and LOLEP. Yields for $1.7 \leq E_\ell \leq 2.0$ are not given.

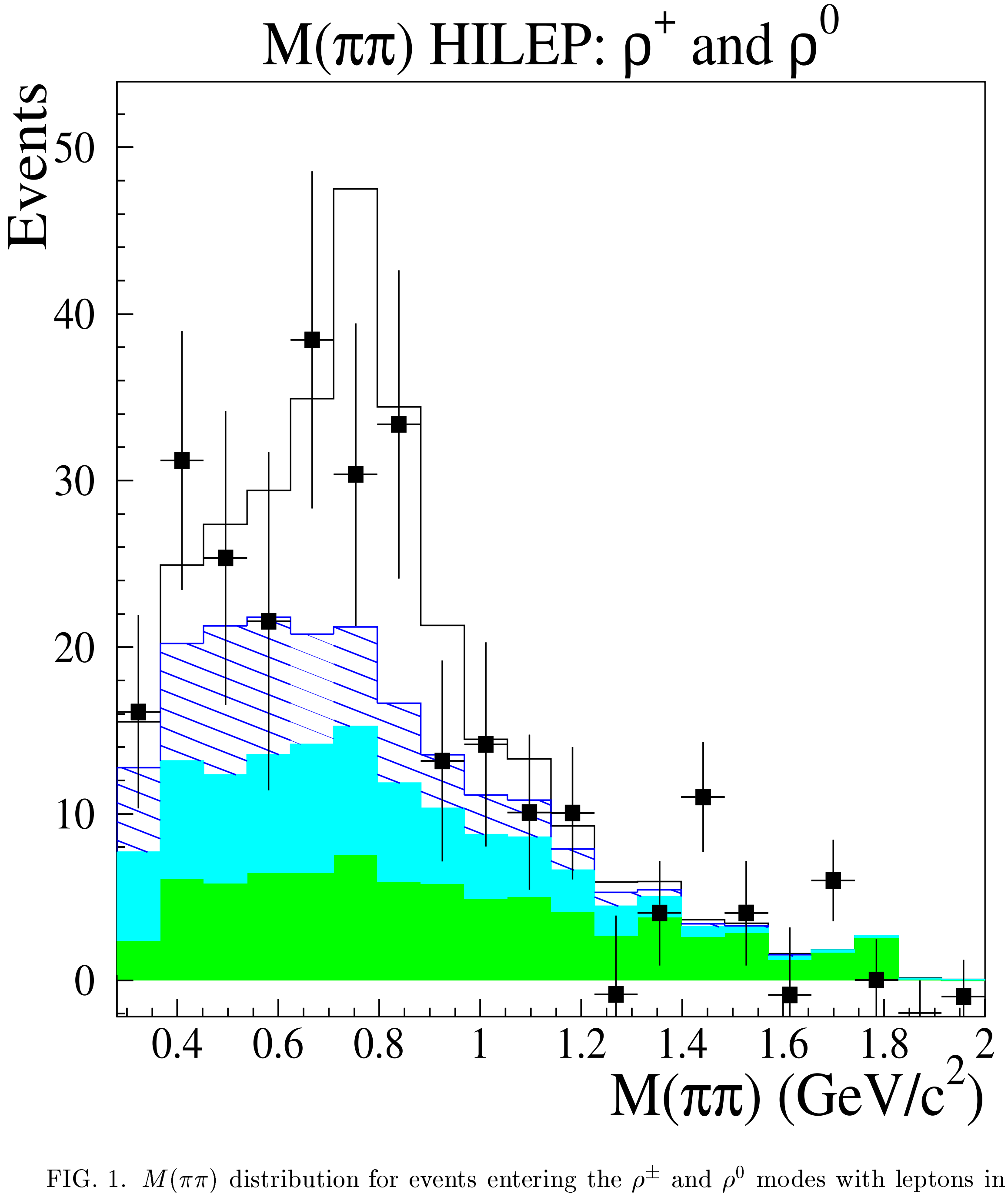

FIG. 1. $M(\pi\pi)$ distribution for events entering the $\rho^{\pm}$ and ρ^0 modes with leptons in HILEP ($2.3 \le E_\ell \le 2.7$ GeV) and $\Delta E \ge -0.2$ GeV. The points are the data after continuum subtraction. The unshaded region shows the contribution from signal events. The hatched region shows the crossfeed contribution. Here the crossfeed contribution includes $\rho^0\ell\nu$ events entering the $\rho^{\pm}\ell\nu$ mode, $\rho^{\pm}\ell\nu$ events entering the $\rho^0\ell\nu$ mode, and $\omega\ell\nu$ events entering the $\rho\ell\nu$ modes. This contribution is considered signal in the fit. The upper (lightly) shaded region is the contribution from $b \to u\ell\nu$ feeddown as well as the contribution from $B \to \pi\ell\nu$ events. The lower (darkly) shaded region is the contribution from $b \to c\ell\nu$ events.

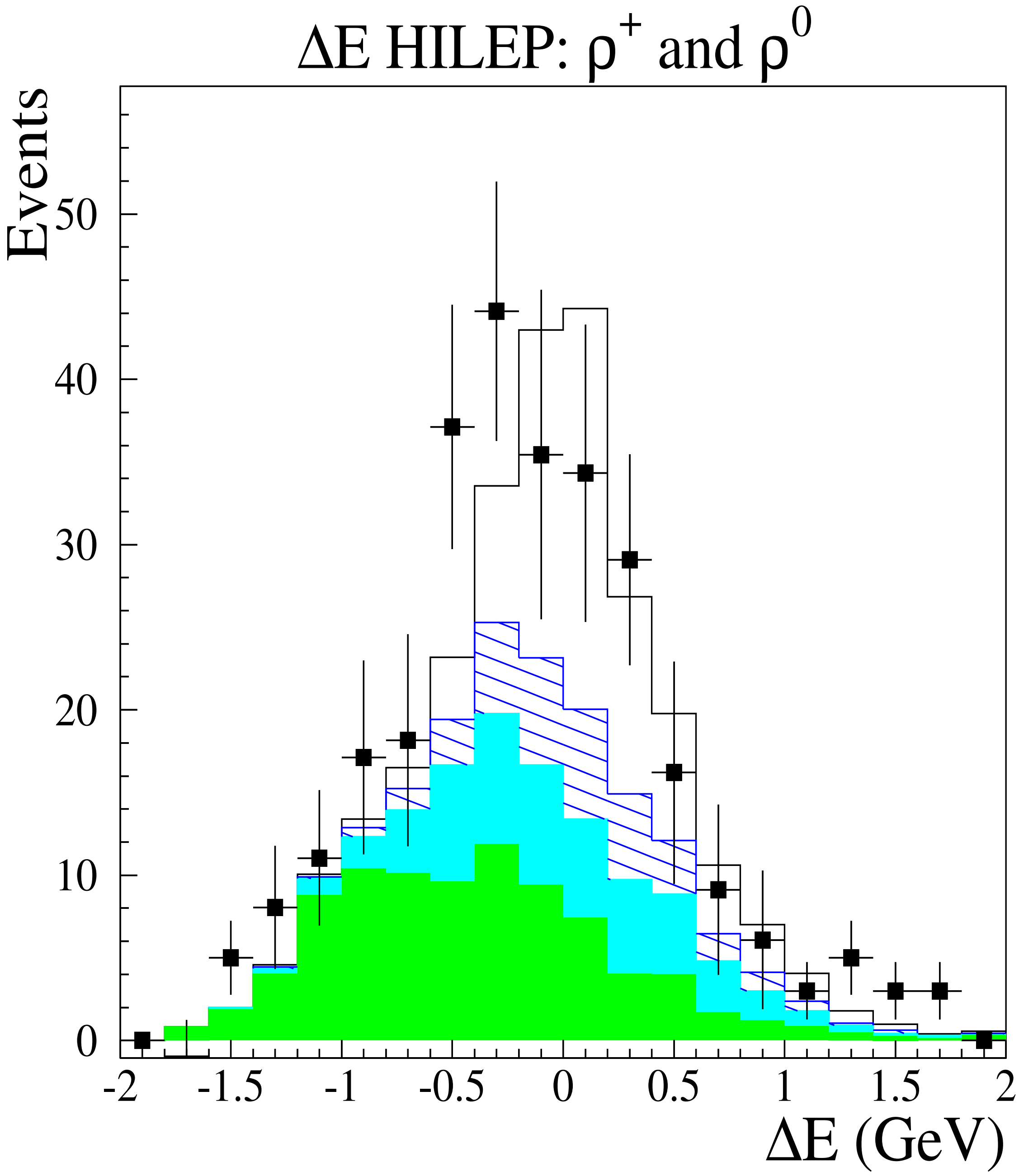

FIG. 2. ΔE distribution for events entering the $\rho^{\pm}$ and ρ^0, modes with leptons in HILEP ($2.3 \leq E_\ell \leq 2.7$ GeV) and with $M(\pi\pi)$ within ± 150 MeV of the nominal ρ mass. The points are the data after continuum subtraction. The shading is described in Figure 1.

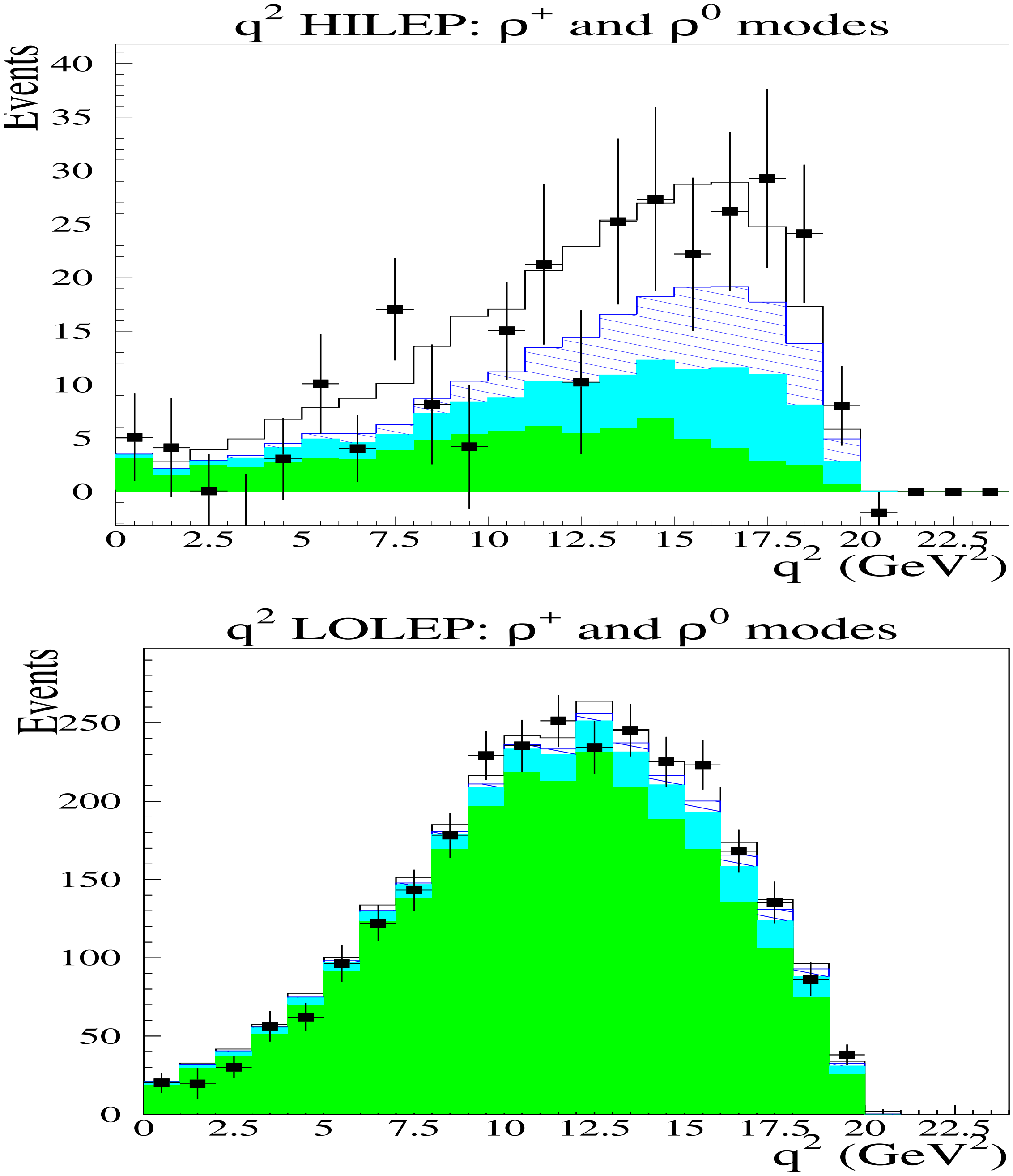

FIG. 3. q^2 distributions for $\rho^{\pm}$ and ρ^0 events in HILEP (top, $2.3 \leq E_\ell \leq 2.7$ GeV) and LOLEP (bottom, $2.0 \leq E_\ell \leq 2.3$ GeV). The points are the data after continuum subtraction. The shading is described in Figure 1.

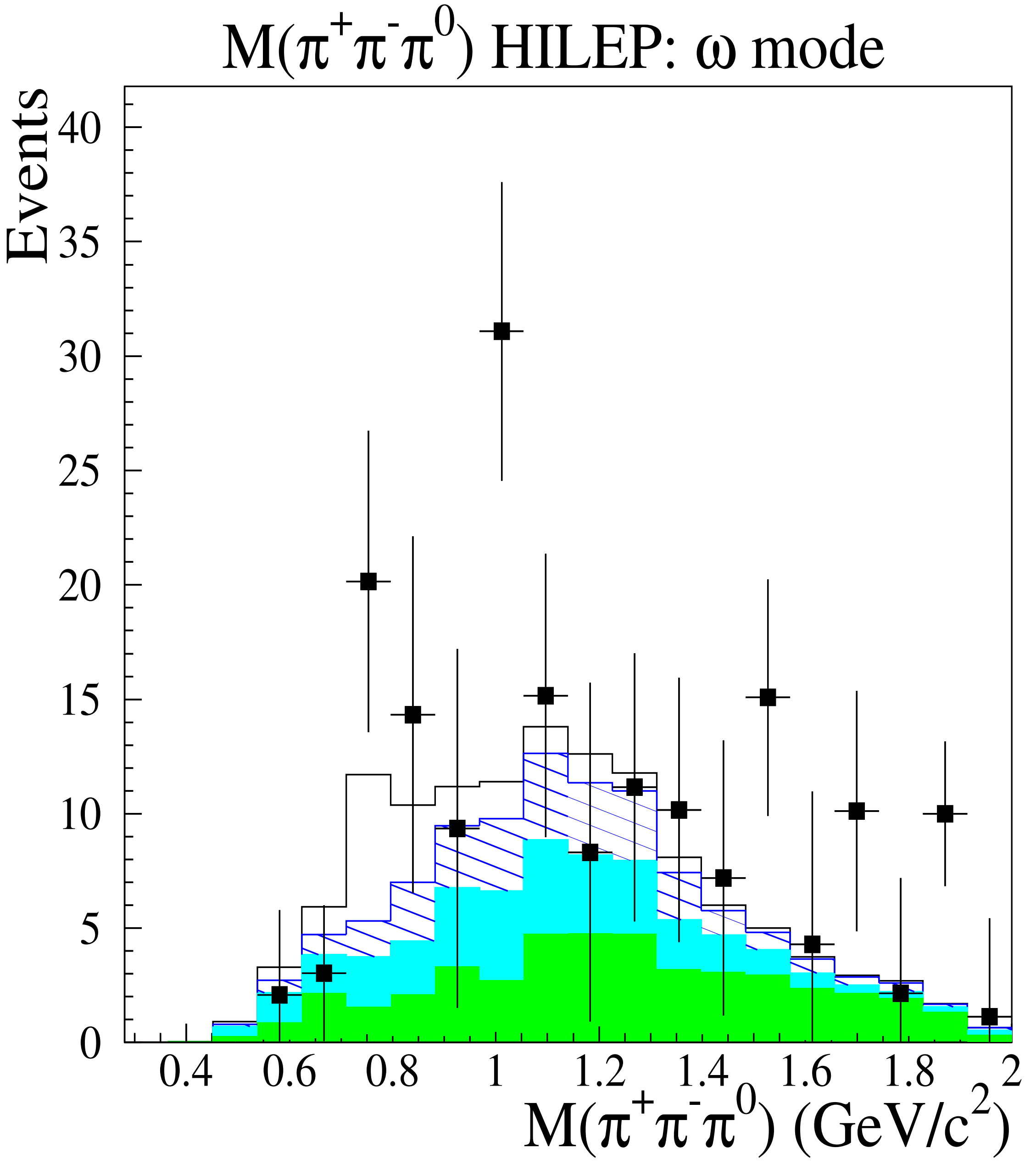

FIG. 4. $M(\pi^+\pi^-\pi^0)$ distribution for events entering the ω mode with leptons in HILEP ($2.3 \leq E_\ell \leq 2.7$ GeV) and $\Delta E \geq -0.2$ GeV. The points are the data after continuum subtraction. The shading is described in Figure 1. Crossfeed into the ω mode consists of $\rho\ell\nu$ events entering the $\omega\ell\nu$ mode.

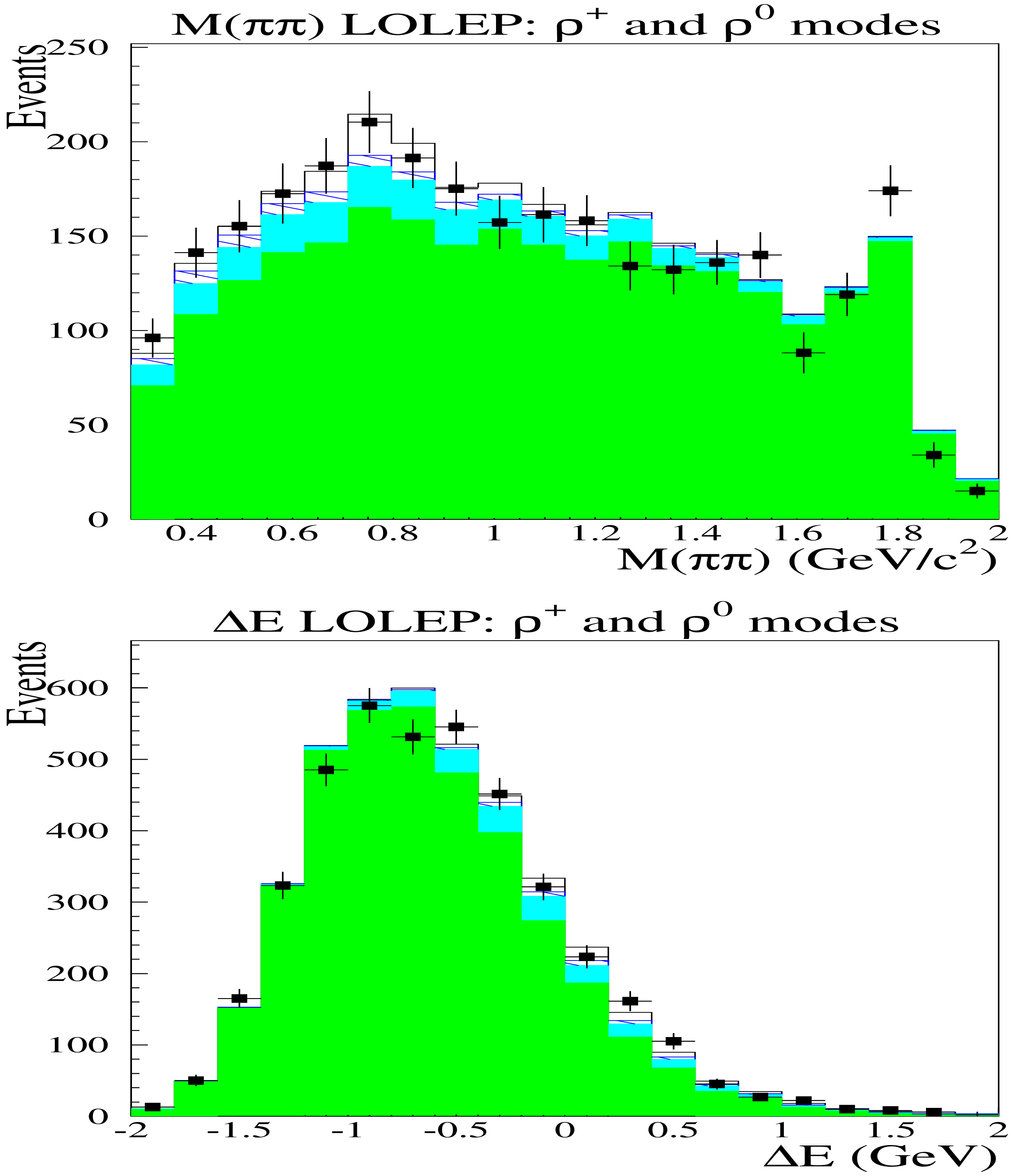

FIG. 5. $M(\pi\pi)$ and ΔE distributions for events in LOLEP ($2.0 \leq E_\ell \leq 2.3$ GeV). The points are the data after continuum subtraction. The shading is described in Figure 1.

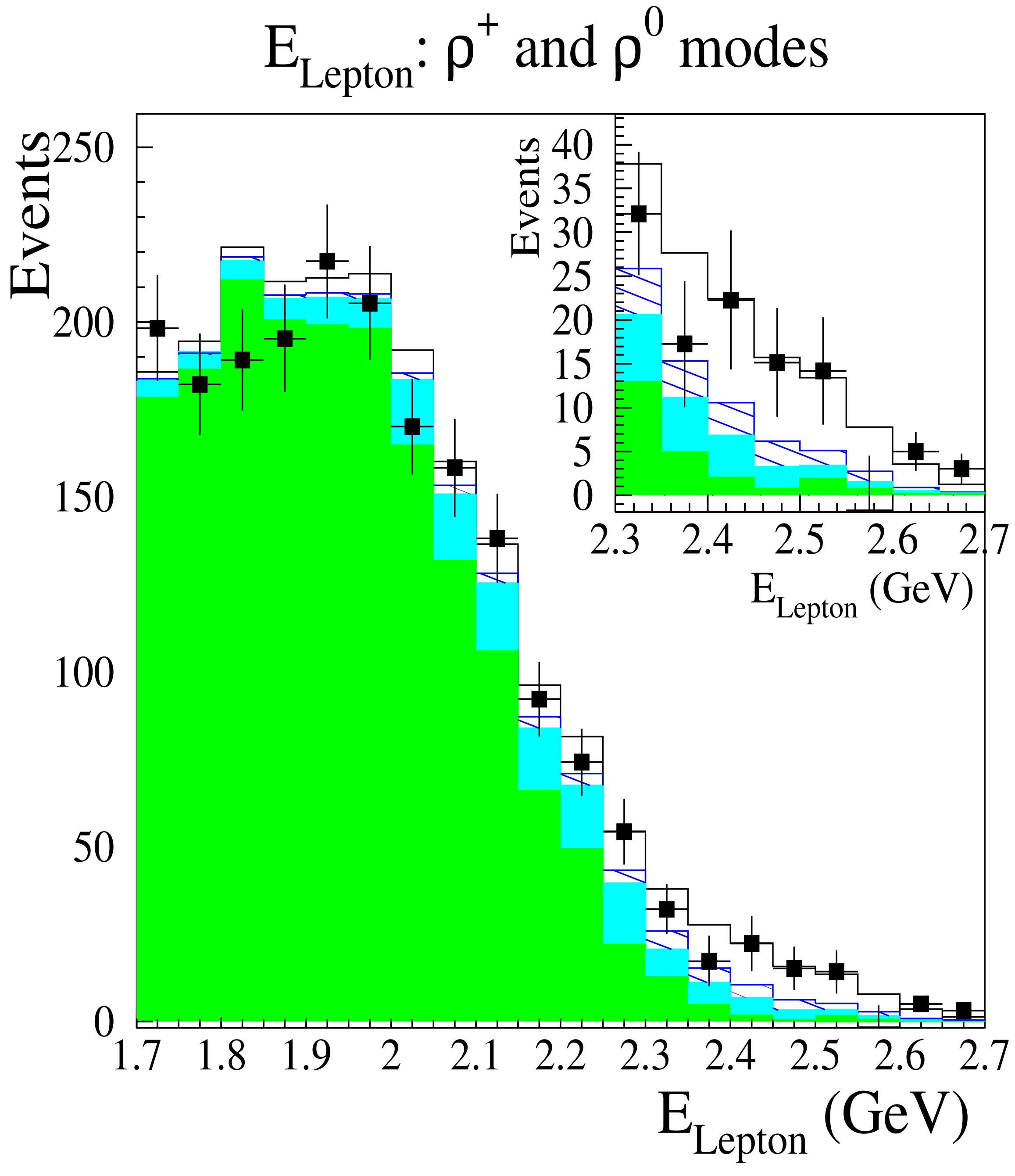

FIG. 6. The lepton energy distribution for events entering the $\rho^{\pm}$ and ρ^0 modes with $\Delta E \geq -0.2$ GeV and $M(\pi\pi)$ within ± 150 MeV of the nominal ρ mass. The points are the data after continuum subtraction. The shading is described in Figure 1.

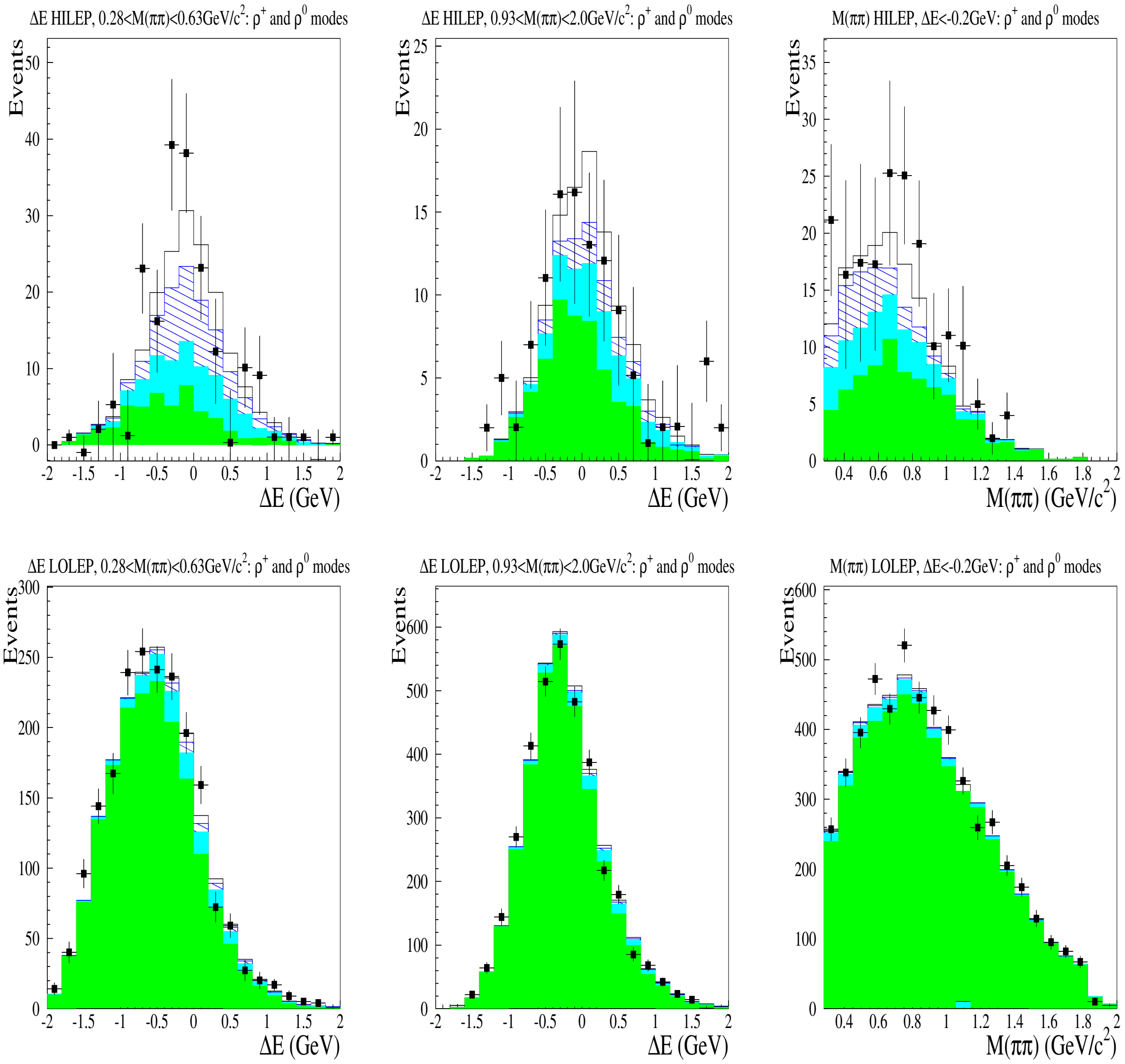

FIG. 7. Shown are projections of the fit in ΔE and $M(\pi\pi)$ where the signal component is expected to be small. The upper set of plots shows results in the HILEP lepton-energy bin, and the lower set is for LOLEP. The left plots show the ΔE distribution for events with $0.28 \leq M(\pi\pi) \leq 0.63$ GeV/c^2. The middle plots show ΔE for events with $0.93 \leq M(\pi\pi) \leq 2.0$ GeV/c^2. The right set of plots shows $M(\pi\pi)$ for $\Delta E \leq -0.2$ GeV. The points are the data after continuum subtraction. The shading is described in Figure 1.

Systematic	$\mathcal{B}_\rho$
Simulation of detector/the other B	11%
$B \to D^{(*)}\ell\nu$ composition	5%
$B \to X_u\ell\nu$ composition	5%
Luminosity	2%
Lepton Identification	2%
Fake lepton rate	2%
$b \to c\ell\nu$ endpoint simulation	5%
Continuum background	5%
Total Systematic error	15%

TABLE II. Summary of systematic errors on the $B \to \rho\ell\nu$ and $B \to \pi\ell\nu$ branching fractions.

VI. SYSTEMATIC ERRORS

Table II shows the breakdown of systematic errors. The largest source of systematic error comes from the Monte Carlo modeling of the detector and of the second B in the event. The ΔE distribution, especially for $b \to c\ell\nu$ events, is affected most. In particular, we have examined our sensitivity to the effects of our track and photon finding efficiencies and momentum resolutions, as well as the modeling of the detector endcaps.

Effects of changing the mix of either $B \to D^{(*)}X\ell\nu$ or $B \to X_u\ell\nu$ feeddown events in the Monte Carlo are relatively small. Allowing a different normalization for the $b \to u\ell\nu$ feeddown in each lepton-energy bin reduces our sensitivity to the modeling of this background.

We have also studied the effects of how the $b \to c\ell\nu$ Monte Carlo is modeled near its lepton-energy endpoint. Although we fit for the normalization of the $b \to c\ell\nu$ component, we rely on the Monte Carlo for the distribution of the lepton-energy spectrum. We see only a small change in $\mathcal{B}(B^0 \to \rho^-\ell^+\nu)$ for large variations of this distribution.

We have not yet evaluated two important sources of systematic error, the effects of $B \to \pi\pi\ell\nu$ nonresonant events, and our model dependence. $B \to \pi^0\pi^0\ell\nu$ is a channel that can only have a nonresonant signal contribution. Our fit agrees well with the data in this mode; however our efficiency for reconstructing a $\pi^0\pi^0$ combination is quite low. As we are primarily sensitive to leptons with energies greater than 2.3 GeV, model dependence is expected to be significant.

VII. INTERPRETATIONS AND CONCLUSIONS

We have reported on preliminary results of a new measurement of the exclusive $b \to u\ell\nu$ modes $B \to \rho\ell\nu$ and $B \to \omega\ell\nu$. We find

$$\mathcal{B}(B^0 \to \rho^-\ell^+\nu) = (2.0 \pm 0.3 \pm 0.3) \times 10^{-4} \qquad \text{(ISGW2)}, \tag{11}$$

using the ISGW2 model for signal efficiencies. We assume no contribution from $B \to \pi\pi\ell\nu$ nonresonant contribution and we have not yet included this effect in our systematic error. As we have not yet evaluated the model dependence of this result, we do not calculate a value for $|V_{ub}|$.

The $\mathcal{B}(B^0 \to \rho^- \ell^+ \nu)$ value reported here is consistent with results previously published by CLEO. Although the event samples are largely independent, systematic, model dependence and statistical correlations have not been been fully evaluated. These numbers are preliminary and should not yet be averaged with previously reported measurements.

REFERENCES

[1] N. Isgur and D. Scora, Phys. Rev. **D52**, 2783 (1995); D. Melikhov, Phys. Rev. **D53**, 2160 (1996).

[2] D. Melikhov, Phys. Lett. **B380**, 363 (1996).

[3] J. M. Flynn *et al.*, Nucl. Phys. **B461**, 327 (1996).

[4] P. Ball, *et al.*, Phys. Rev. **D55**, 5561 (1997).

[5] J. P. Alexander *et al.*, Phys. Rev. Lett. **77**, 5000 (1996).

[6] G. C. Fox and S. Wolfram, Phys. Rev. Lett. **41** 1581 (1978).

[7] R. A. Fisher, Annals of Eugenics, **7**, 179 (1936).

[8] Y. Kubota *et al.*, Nucl. Instrum. Methods Phys. Res. **A320**, 66 (1992).

[9] J. L. Diaz-Cruz *et al.*, Phys. Rev. **D54**, 2388 (1996), have computed isospin corrections due to ρ-ω mixing.

[10] R. Brun *et al.*, GEANT 3.15, CERN DD/EE/84-1.

[11] F. James, CERN Program Library Long Writeup D506, Mar. 1994.